Off-Grid Perfect Boundary Conditions for the FDTD Method

Yotka S. Rickard, *Member, IEEE,* and Natalia K. Nikolova, *Member, IEEE*

***Abstract*—We implement off-grid boundary conditions within Yee's finite-difference time-domain (FDTD) method without disturbing the existing uniform mesh or changing the standard FDTD code. Both perfect electric conductor and perfect magnetic conductor walls are considered. Examples of straight, slanted, and curved walls are shown, the latter two being represented by an enhanced staircase approximation. We show that: 1) offsets comparable to the spatial step size lead to instabilities and 2) this issue is easily resolved by stepping into the neighboring cell. The method enhances the flexibility of the FDTD method with respect to complex geometrical domains without reducing the spatial step.**

***Index Terms*—Finite-difference time-domain (FDTD) methods, off-grid boundary conditions (BCs), slanted and curved boundaries.**

I. Introduction

In THE finite-difference time-domain (FDTD) method [1], for good spatial resolution, the spatial step is usually chosen between 5%–12.5% of the minimal wavelength of interest. However, in many structures, it may not be possible to position the boundaries at integer multiples of the chosen spatial step. The usual way to handle such structures is to reduce the spatial step or to use a nonuniform grid [2]. The first option leads to an increase in the computational load. The second one lowers the accuracy, requires reduction of the time step, and may lead to late-time instabilities.

Offset planar or curved metal boundaries have also been treated by few FDTD modifications. These include locally conformal methods (compared in [3]) such as the conformal finite-difference time-domain (C-FDTD) [4] and the contour-path finite-difference time-domain (CP-FDTD) [5] methods, as well as methods using new FDTD formulations [6] or sub-cell models [7]. All these require changes in the existing FDTD code, some of them substantial, as well as changes in the grid and time step.

We propose an alternative to the above options, whereby the boundaries may be described without disturbing the original (coarse, uniform) spatial grid. The method employs extrapolation of adjacent field values from the internal computational domain to obtain exterior (auxiliary) field values ensuring off-grid virtual boundaries in between, as in [8]. The proposed off-grid boundaries are applicable in modeling parallel, slanted, and curved walls with respect to the existing grid. This significantly enhances the flexibility of the FDTD method with respect to complex geometrical shapes. In the proposed approach, the modifications concern only the outer boundary values of the tangential electric-field components, as is usually the case with Yee's algorithm. Moreover, the existing conventional FDTD code and the grid remain unchanged. Time-step reduction is unnecessary, thus, the high speed of the computations is preserved. The memory requirements are practically unchanged.

In the FDTD method, metal walls are usually considered to be perfect electric conductors (PECs). In general, PEC walls can be described mathematically in two ways: 1) either as vanishing tangential electric-field components, which is a Dirichlet boundary condition (BC) or 2) as vanishing normal derivatives of the tangential magnetic-field components, which is a Neumann BC.

Similarly, when symmetry is present, a perfect magnetic conductor (PMC) wall may be employed to reduce the computational load. It is mathematically represented by either vanishing normal derivatives of the tangential electric-field components, Neumann BC, or vanishing tangential magnetic-field components, Dirichlet BC. Therefore, theoretically we may describe all on- or off-grid virtual perfect BCs in terms of either Dirichlet or Neumann BCs.

The FDTD method based on Yee's discretization of Maxwell's equations [1] assumes that the field variation between the grid nodes is linear. Therefore, a linear extrapolation of the field values is used in the derivation of off-grid Dirichlet BC. Correspondingly, a quadratic extrapolation of the field values for off-grid Neumann BC is used (the latter being linear with respect to the field derivatives).

To validate the proposed method, the resonant frequency for the first few resonant modes of a rectangular resonator are compared to their analytical values when the resonator is slid with respect to and in parallel with the existing grid by noninteger number of cells. A comparison of the proposed algorithm with the nonuniform FDTD method is shown. Displacements of PEC and PMC walls are considered.

Examples of modeling slanted walls are also shown. A rectangular resonator is rotated while the existing grid is kept stationary. The proposed off-grid BCs are used to modify the conventional staircase approximation of the slanted boundary walls and to significantly improve its accuracy. In the presented examples, the slanted walls are misaligned with respect to the grid in two dimensions. It is straightforward to extend the method to three-dimensional misalignments. The resonant frequency for

Manuscript received June 19, 2004; revised February 24,2005. This work was supported by the Natural Sciences and Engineering Research Council of Canada and by the Canadian Space Agency fellowship supplement under a Post-Doctoral Fellowship.

The authors are with the Department of Electrical and Computer Engineering, McMaster University, Hamilton, ON, Canada L8S 4K1 (e-mail: yotka@ece.mcmaster.ca; talia@mcmaster.ca).

Digital Object Identifier 10.1109/TMTT.2005.850457

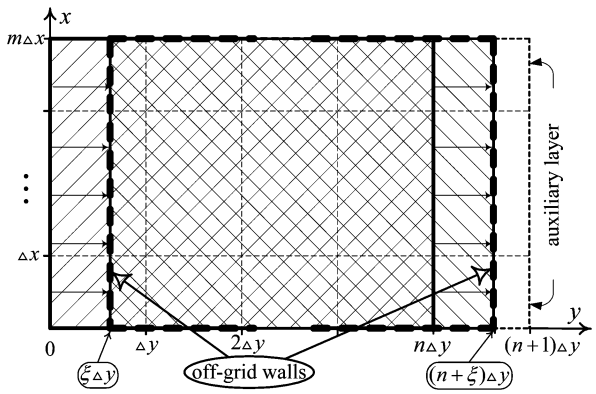

Fig. 1. Geometry of the cross section of the original rectangular cavity and its modified version displaced in the positive y-direction by $\xi\,\Delta y$.

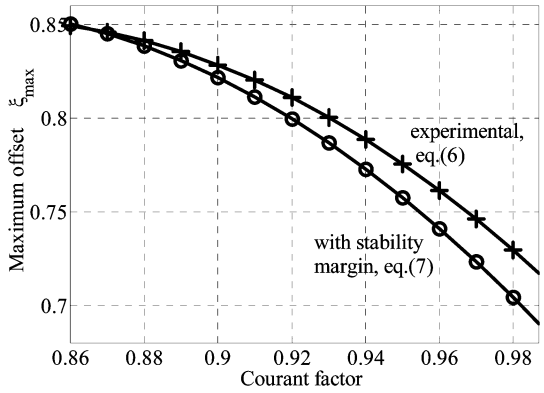

Fig. 2. Dependence of the maximum offset on the time step via Courant factor.

the dominant mode and the next few resonant modes are compared to their analytical values and to the values obtained before the rotations.

Finally, an example of modeling the curved walls of a cylindrical resonator is shown using our new staircase approximation. In all examples, excellent accuracy is obtained. Beside the accuracy, we also investigate the stability with our off-grid BC and give recommendations accordingly. In the Appendix, the algorithm for the implementation of the off-grid BC for slanted walls is outlined.

II. Off-Grid Dirichlet BC

First, the modeling of the off-grid Dirichlet BC at PEC walls that are in parallel with the existing grid, but do not coincide with the grid layers, is explored.

Consider a rectangular resonator, modeled by the FDTD method on a uniform grid of a spatial step $\Delta x = \Delta y = \Delta z$. While the original grid is kept stationary, the structure of size ($m\Delta x$, $n\Delta y$, $k\Delta z$) is moved in the positive y-direction by $\xi\Delta y$, $\xi \in (0,1)$, as shown in Fig. 1.

As ξ is not an integer, the PEC walls perpendicular to the y-direction now have off-grid locations. Using the original grid, a virtual PEC wall at $y^* = \xi\Delta y$ can be modeled as described below.

For brevity, any electric-field component tangential to the PEC wall is denoted by $E_t(x,y,z) = f(y)$, and its grid values are $f(k\Delta y) = f_k$, $k = 0,\ldots,n+1$. Assuming a linear variation between adjacent layers and using the function values

$$\begin{aligned} \text{at } \Delta y, \qquad & f(\Delta y) = f_1 = a\Delta y + b \\ \text{at } \xi\Delta y, \qquad & f(\xi\Delta y) = 0 = a\xi\Delta y + b \end{aligned} \tag{1}$$

we arrive at

$$f(y) = \frac{f_1}{1-\xi}\left(\frac{y}{\Delta y} - \xi\right). \tag{2}$$

In particular, the values assigned to the left-most layer at $y = 0$ are

$$f_0 = f(0) = \left(\frac{\xi}{\xi - 1}\right) f_1, \qquad \xi \le \xi_{\max}. \tag{3}$$

Clearly, the f_0 layer is external to the computational domain.

Similarly, at the right end, the virtual off-grid PEC wall is at $y^* = (n+\xi)\Delta y$ and the field values of an auxiliary (additional) layer at $(n+1)\Delta y$ can be expressed in terms of the known field values from the layer at $n\Delta y$ as

$$f_{n+1} = \left(\frac{\xi - 1}{\xi}\right) f_n, \qquad \xi \ge 1 - \xi_{\max}. \tag{4}$$

Notice that the coefficients in (3) and (4) correspond to the slopes of the approximating lines and, thus, grow to infinity when the offset boundary approaches the internal grid layer. This affects the stability. Therefore, an upper limit $\xi_{\max}$ in (3) and a lower limit $\xi_{\min} = 1 - \xi_{\max}$ in (4) are imposed. The maximum offset $\xi_{\max}$ depends on the Courant factor c_{CFL} from the time-step definition, which, for uniform grids, is (see, e.g., [2])

$$\Delta t = \frac{c_{\mathrm{CFL}}\Delta x}{\sqrt{3}}\sqrt{\mu\varepsilon}. \tag{5}$$

The upper curve in Fig. 2 shows the experimentally obtained interdependence between c_{CFL} and $\xi_{\max}$, which can be approximated as

$$c_{\mathrm{CFL}} = -4.775\xi_{\max}^2 + 6.6\xi_{\max} - 1.294. \tag{6}$$

In practice, the maximum offset is calculated based on the user-defined coefficient c_{CFL}. For numerical stability, we propose approximately 2% lower margin for the maximum offset at the high end of practical values of c_{CFL}, which leads to

$$\xi_{\max} = 0.643 + 0.584\sqrt{1 - 1.01 \cdot c_{\mathrm{CFL}}}. \tag{7}$$

It is shown as the lower curve in Fig. 2. From Fig. 2, the practical range of the c_{CFL} values ($0.866 \le c_{\mathrm{CFL}} \le 0.98625$) corresponds to maximum offsets between $0.85 \ge \xi_{\max} \ge 0.7$ in (3) and (4). Offsets $\xi > \xi_{\max}$ are dealt with as follows.

For a virtual off-grid PEC wall at $y^* = \xi\Delta y$, (3) can be generalized so that the field value at the leftmost layer at $y = 0$ is expressed through the field value at a further neighbor $s\Delta y$ as

$$f_0 = f_s\left(\frac{\xi}{\xi - s}\right), \qquad s = 1,2,3\ldots. \tag{8}$$

Similarly, for a virtual off-grid PEC wall at $y^* = (n+\xi)\Delta y$, (4) can be generalized so that the field value of the right-most

auxiliary layer at $(n+1)\Delta y$ is expressed in terms of the known field values from the layer at $(n+1-s)\Delta y$ as

$$f_{n+1} = f_{n+1-s}\left(\frac{1-\xi}{1-\xi-s}\right), \qquad s = 1, 2, 3 \ldots. \tag{9}$$

Formulas (8) and (9) with $s = 2$ are used in two cases, which are: 1) if the offset $\xi > \xi_{\max}$ in (3) or $\xi < \xi_{\min}$ in (4), and 2) if the closest neighboring field value is zero, which happens in modeling slanted and curved walls.

One may notice that (4) and (9) are actually the same as (3) and (8), respectively, when

$$\xi_{\text{right}} = 1 - \xi_{\text{left}}. \tag{10}$$

Therefore, (3) and (8) may be used for both left- and right-hand-side off-grid Dirichlet BCs if the offset ξ is always measured from the external layer to the off-grid boundary.

An alternative to (8) is to use a weighted sum of f_1 and f_2

$$f_0 = [(1-\xi_w)f_1 + \xi_w f_2]\left(\frac{-\xi}{1-\xi+\xi_w}\right), \qquad 0 \le \xi \le 1 \tag{11}$$

where $\xi_w = |\xi - \xi_{\max}|$ defines the position of the weighted sum between f_1 and f_2. The advantages of using (11) are as follows.

1) It holds for all offsets, the dependence on $\xi_{\max}$ is embedded in the formula, and thus, the explicit switch of $s = 1$ with $s = 2$ for $\xi > \xi_{\max}$ in (8) is avoided.
2) It is numerically stable because the denominator is limited from below $|1 - \xi - \xi_w| \ge 1 - \xi_{\max}$.
3) It leads to better accuracy, especially on coarse grids, as shown in Section IV-A. If the grid is not coarse, (8) and (11) lead to practically the same result.
4) It holds regardless of the value of f_1 (including $f_1 = 0$), which is convenient in slanted-wall applications.

It is important to note that the proposed algorithm is not equivalent to the common nonuniform FDTD: our space–time grid is preserved uniform for both the $\mathbf{E}$- and $\mathbf{H}$-field components, the stability conditions are thus different; the implementation of staircase approximations is different, and, finally, the numerical results exhibit differences as well.

III. Off-Grid Neumann BC

When modeling Neumann BCs, without restricting ourselves, we can think of a PMC wall modeled as vanishing normal derivatives of the tangential electric-field components. Similar to the PEC-wall case, off-grid PMC walls can be modeled without disturbing the existing mesh. Keeping the grid stationary, when a PMC wall is moved in the positive y-direction by $\xi\Delta y$, $\xi \in (0, 1)$, Neumann BC is applied at the off-grid position $\xi\Delta y$

$$\frac{\partial f(\xi\Delta y)}{\partial y} = 0. \tag{12}$$

A linear variation with respect to this derivative requires the use of a quadratic variation of the tangential-field values $f(y)$ between adjacent layers. Thus,

$$\begin{aligned} \text{at } \Delta y, &\quad f(\Delta y) = f_1 = a(\Delta y)^2 + b\Delta y + c \\ \text{at } 2\Delta y, &\quad f(2\Delta y) = f_2 = a(2\Delta y)^2 + b(2\Delta y) + c \\ \text{at } \xi\Delta y, &\quad \frac{\partial f(\xi\Delta y)}{\partial y} = 0 = 2a(\xi\Delta y) + b. \end{aligned} \tag{13}$$

Eliminating a, b, and c from (13), for a virtual PMC wall at $y^* = \xi\Delta y$, we obtain

$$f(y) = \frac{1}{(3-2\xi)}\left[(f_2 - f_1)\left(\frac{y}{\Delta y}\right)^2 + 2\xi(f_2 - f_1)\left(\frac{y}{\Delta y}\right) + (2\xi - 1)f_2 + 4(1-\xi)f_1\right]. \tag{14}$$

In particular, we assign for the left-most layer at $y = 0$,

$$f_0 = f_1 + (f_2 - f_1)\left(\frac{2\xi - 1}{3 - 2\xi}\right). \tag{15}$$

Similarly, for a virtual right-end PMC wall at $y^* = (n+\xi)\Delta y$, the tangential electric-field values of the additional layer at $(n+1)\Delta y$ are expressed as

$$f_{n+1} = f_n + (f_n - f_{n-1})\left(\frac{2\xi - 1}{2\xi + 1}\right). \tag{16}$$

The same argument as with the offset (10) holds for the left- and right-hand-side off-grid Neumann BC. Thus, (15) may be used in all cases of off-grid Neumann BCs if the offset ξ is always measured from the external layer to the off-grid boundary.

IV. Validation and Discussion

A. Modeling of Off-Grid Dirichlet BC

To validate the proposed method, we have implemented it in a standard FDTD code and computed the first few resonant frequencies of a rectangular cavity of dimensions $h = 10$ mm, $w = 20$ mm, and $L = 30$ mm, shown in Fig. 3. The relative error is calculated as

$$\delta = \left|\frac{f_{\text{reference}} - f_{\text{approx}}}{f_{\text{reference}}}\right| \times 100\%. \tag{17}$$

The excitation is a sine wave of 12 GHz modulated by a Blackman–Harris window (BHW) function [9]. Firstly, the resonator has been modeled by the standard FDTD algorithm on a uniform grid of $\Delta x = \Delta y = \Delta z = 1$ mm with $c_{\text{CFL}} = 0.866$ in (5). From (7), this leads to $\xi_{\max} = 0.85$. The first few resonant frequencies and their relative errors with respect to the analytical values have been calculated. The frequency step of the fast Fourier transform (FFT) is $\Delta f = 5 \times 10^{-4}$ GHz. Keeping the grid stationary, the resonator has then been slid in the positive y-direction by $\xi\Delta y$ for ξ from 0.05 to 0.95 with increments of 0.05. In addition, around the switch points $\xi = 0.15$ and $\xi = 0.85$, increments of $\pm$ 0.0001, 0.001, and 0.01, as well as offsets of 0.01, 0.001, and 0.0001 from both ends are used. The off-grid (left- and right-hand side) PEC boundaries have been

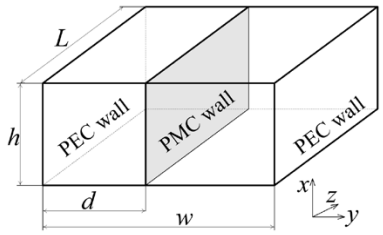

Fig. 3. Geometry of the rectangular resonator. All outer walls are PEC walls. For the off-grid Dirichlet BC experiment, the whole structure is simulated. For the off-grid Neumann BC experiment, half of the structure is simulated, terminated by a PMC wall at $d = 0.5w$.

TABLE I
RELATIVE ERRORS OF THE MODAL RESONANT FREQUENCIES WITH ON- AND OFF-GRID PEC WALLS

	On-grid ($\xi = 0$)		Off-grid ($0.001 \le \xi \le 0.999$)	
Analytical [GHz]	Calculated [GHz]	δ [%]	Calculated [GHz]	δ [%]
$f_{011} = 9.007642$	9.00337	0.0475	9.00337	0.0475
$f_{012} = 12.491352$	12.48090	0.0832	12.48096	0.0832
$f_{101} = 15.800450$	15.75949	0.2592	15.75949	0.2592
$f_{110} = 16.758908$	16.72182	0.2213	16.72182	0.2213
$f_{111} = 17.487893$	17.45572	0.1840	17.45572	0.1840

modeled by the off-grid Dirichlet BC, as described in Section II: using (8) with $s = 1$ for $\xi \le 0.85$ and with $s = 2$ for $\xi > 0.85$, where ξ is measured always from the external layer to the offset boundary. The results with on- and off-grid boundaries for the dominant resonant mode TE_{011} and for the next few resonant modes are compared with their analytical values in Table I. It is seen that the calculated frequencies with off-grid Dirichlet BCs are indistinguishable from those obtained with the on-grid structure.

Here, it is important to note that the time step has not been changed from its original value.

Next, experiments are conducted where the resonator is slid in the positive x-direction and, finally, in both x- and y-directions at the same time. In all cases, the resultant frequency is exactly the same as for the initial structure with on-grid PEC walls. With a coarser mesh of $\Delta x = \Delta y = \Delta z = 2$ mm, the relative error for the frequency of the TE_{011} mode with on-grid PEC walls is 0.18%. The application of the off-grid Dirichlet BC again gives exactly the same values for the TE_{011} frequency and for the next few resonant frequencies as with the on-grid PEC BC.

Although 30 000 time steps are more than enough to obtain the resonant frequencies with sufficient accuracy from the time-domain response, simulations with 200 000 time steps have been performed. No late-time instabilities have been observed in the range $0.00001 \le \xi \le 0.99999$.

Finally, to explore the dependence of the accuracy of the calculated resonant frequencies on the offset, only the left PEC wall of the resonator from Fig. 3 has been shifted. The simulation is purposefully made coarse by choosing a grid of $\Delta x = \Delta y = \Delta z = 2$ mm and a Courant factor in (5) as $c_{\mathrm{CFL}} = 0.98625$. In this case, as per Fig. 2, $\xi_{\max} = 0.7$. Approximately 2% reduction, as proposed in (7), yields

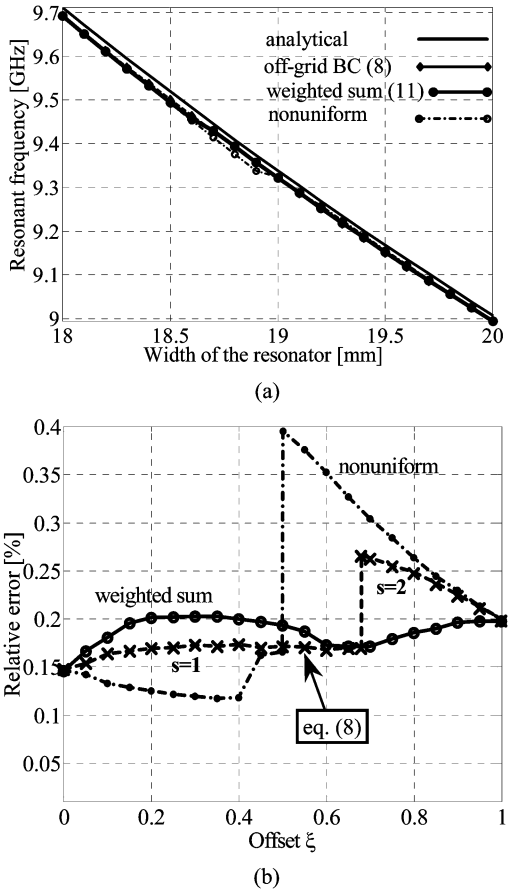

Fig. 4. Variation of the first resonant frequency with respect to the displacement ξ when only the left-hand-side PEC wall is shifted. (a) Comparison of the calculated and analytical results. (b) Relative errors in the calculated frequencies with respect to their analytical values when the off-grid BCs [see (8) and (11)] are used and when a nonuniform left-most layer is used.

$\xi_{\max} = 0.6794$, and this is the switch value used in (8). The first few resonant frequencies have been calculated using: 1) the proposed off-grid Dirichlet BCs (8) and (11), and 2) a nonuniform first layer. The calculated results for the first resonant frequency are compared with the analytical values in Fig. 4(a). To preserve the stability for any displacement with the off-grid BC, $s = 1$ in (8) is used for $0 \le \xi \le \xi_{\max}$, and $s = 2$ for $\xi > \xi_{\max}$. The weighted sum (11) holds for any displacement. The nonuniform FDTD with $c_{\mathrm{CFL}} = 0.98$ is stable up to $\xi_{\max} = 0.5$, where the nonuniform first layer for $0 \le \xi \le 0.5$ has a width $(1-\xi)\Delta y$. For offsets $\xi > 0.5$, the first (narrow) layer is merged with the second layer to form a cell width of $(2-\xi)\Delta y$. The initial $(\xi = 0)$ and the final $(\xi = 1)$ offsets are modeled with an on-grid PEC BC. The difference in the accuracy of the two methods can be seen in more detail through their relative errors with respect to the respective analytical solutions, as shown in Fig. 4(b). Note that the jump in the calculated frequency (at the corresponding switch point) for the nonuniform case is much bigger than the jump when $s = 2$ replaces $s = 1$ in (8). Moreover, when using the weighted sum (11) for any $0 \le \xi \le 1$, the slopes of the analytical line and the calculated curve using an off-grid BC are approximately the same for all offsets within the error of the FFT calculation. Using a nonuniform first layer, although it may seem similar, does not give such a smooth result.

TABLE II
RELATIVE ERRORS OF THE MODAL RESONANT FREQUENCIES WITH ON- AND OFF-GRID (LEFT) PEC AND (RIGHT) PMC WALLS

		On-grid BC: ($\xi = 0$)		Off-grid BC: ($\xi = 0.15$)	
Analytical [GHz]	PMC formula	Calculated [GHz]	δ [%]	Calculated [GHz]	δ [%]
$f_{011} = 9.007642$	N1	9.00337	0.048	9.00277	0.054
	N2	9.00696	0.008		
$f_{012} = 12.491352$	N1	12.48096	0.083	12.48096	0.083
	N2	12.48396	0.059		
$f_{110} = 16.758909$	N1	16.72183	0.221	16.72183	0.221
	N2	16.72362	0.211		
$f_{111} = 17.487894$	N1	17.45572	0.179	17.45512	0.182
	N2	17.45752	0.169		

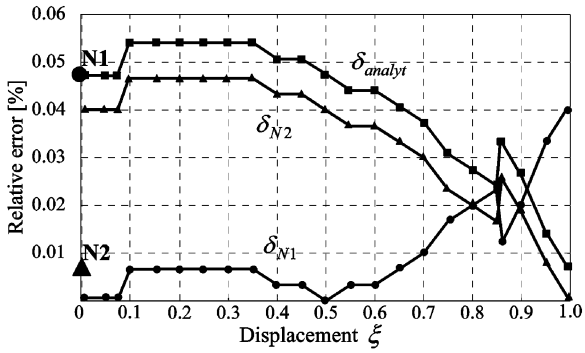

Fig. 5. Relative errors in the frequency of the dominant resonant mode TE_{011} for the rectangular resonator terminated by a PMC wall at the symmetry plane. The off-grid (*left*) Dirichlet and off-grid (*right*) Neumann BCs are applied at a distance $\xi\Delta y$ with respect to their initial (on-grid) positions. The relative errors with on-grid boundaries using a Neumann BC [see (18) and (19)] are shown as big dot $N1$ and big triangle $N2$, respectively.

The above experiment with the same coarse grid and Courant factors $c_{\mathrm{CFL}} = 0.86$ to 0.88, leads to $\xi_{\max} = 0.85$ for the off-grid BC and $\xi_{\max} = 0.65$ for the nonuniform FDTD. The pattern of the relative errors is the same as the one shown in Fig. 4(b) with the exception that the results produced by (8) are almost the same as those of (11). With the nonuniform first layer, the big jump remains almost the same as the one shown in Fig. 4(b), only shifted close to $\xi_{\max} = 0.65$. If a finer grid of $\Delta x = \Delta y = \Delta z = 1$ mm is used, no jump is observed around the switch point of (8); while the result from the nonuniform FDTD retains the jump.

B. Modeling of Off-Grid Neumann BCs

To investigate the accuracy of the off-grid Neumann BC, the same resonator as above has been modeled with a symmetry wall at the plane $y = 0.5w$, as shown in Fig. 3. Initially, the on-grid PMC wall at $n\Delta y$ is modeled by applying the Neumann BC to the tangential electric-field components. This is implemented numerically either as

$$f_{n+1} = f_{n-1} \tag{18}$$

or as

$$f_n = \frac{(4f_{n-1} - f_{n-2})}{3}. \tag{19}$$

Both approximations are of second-order accuracy. In the following, for brevity, approximation (18) is referred to as $N1$ and approximation (19) as $N2$.

The spatial step is $\Delta x = \Delta y = \Delta z = 1$ mm, $c_{\mathrm{CFL}} = 0.88$, and the excitation is the same as above. The first few resonant frequencies are calculated with on-grid boundaries using either $N1$ or $N2$. Their relative errors with respect to the analytical values are summarized in Table II. Leaving the grid stationary, the half-resonator has then been slid in the positive y-direction by $\xi\Delta y$, $\xi \in [0.0001, 0.9999]$ with the same increments as in Section IV-A. The off-grid Neumann BC is applied to the right-hand-side PMC wall, and the off-grid Dirichlet BC is applied to the left-hand-side PEC wall using (16) and (8), respectively. The frequencies of the first few resonant modes have been calculated again (see Table II). In Fig. 5, the relative error of the computed dominant resonant frequency f_{011} using the off-grid BCs is plotted versus the normalized displacement ξ. The relative errors for the shifted resonator with off-grid BCs are calculated with respect to: 1) the analytical value of f_{011}—denoted as δ_{analyt}; 2) the calculated value of f_{011} with $N1$ [on-grid Neumann BC (18)]—denoted as δ_{N1}; and 3) the calculated value of f_{011} with $N2$ [on-grid Neumann BC (19)]—denoted as δ_{N2}.

As Fig. 5 shows, the relative error in the calculations with offset boundaries is practically the same as the error with on-grid BCs. Note that the calculations with off-grid BCs give results very close to the reference result obtained with $N1$ [the on-grid BC (18)]. The error curves δ_{analyt} and δ_{N2} are very close to each other because the reference result with $N2$ [the on-grid BC (19)] is very close to the analytical value. The results for the next few resonant modes repeat the patterns shown in Fig. 5, and the relative errors with on- and off-grid BCs are approximately the same.

C. Modeling of Slanted PEC Walls

The applicability and accuracy of the proposed method in modeling slanted PEC walls has been investigated by the following experiment. The rectangular cavity of Fig. 3 has been rotated, as shown in Fig. 6. The slanted PEC walls are modeled by a conventional staircase (referred to as Case A) and by a modified staircase applying the off-grid Dirichlet BCs.

First, the resonator of dimensions $h = 10$ mm, $w = 15$ mm, and $L = 20$ mm is modeled by the standard FDTD algorithm on a uniform grid of $\Delta x = \Delta y = \Delta z = 1.25$ mm and $c_{\mathrm{CFL}} = 0.866$. The walls of the resonator are kept aligned with the grid. The calculated result (no rotation, on-grid BCs) for the lowest resonant frequency $f_{\mathrm{TE}_{011}} = 12.4752035$ GHz has a relative error of 0.13% with respect to its analytical value.

Keeping the grid stationary, the resonator has then been rotated by 30° in parallel with the plane $x0y$ around the z-axis.

In the following, all cells, which are partially inside and partially outside the actual boundary, are referred to as boundary cells. In the FDTD method, these boundary cells are either excluded or included in the conventional staircase approximations depending on the percentage of their volume inside the cavity. The usual rule-of-thumb is to include these boundary cells, half or more of whose volume is in the interior.

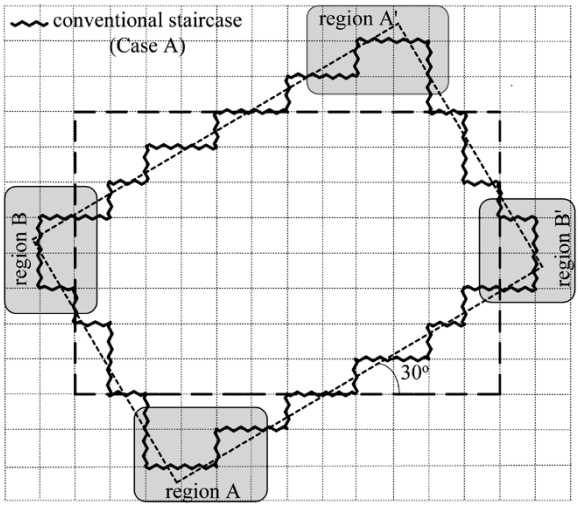

Fig. 6. Rotated rectangular resonator and its (conventional) staircase approximation referred to as Case A.

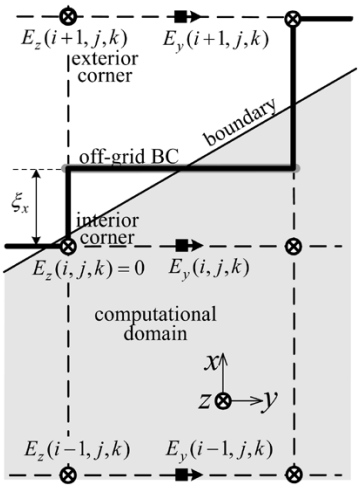

Fig. 7. Numerical cell showing the application of single-face off-grid BCs for a staircase approximation. The component $E_y(i+1,j,k)$ is expressed through $E_y(i,j,k)$ using (9) with $i=n$, $s=1$, and $\xi=\xi_x$. The component $E_z(i+1,j,k)$ is expressed through $E_z(i-1,j,k)$ using (9) with $i=n$, $s=2$, and $\xi=\xi_x$.

1) Versions of Off-Grid Dirichlet BC for Slanted Walls: The application of an off-grid Dirichlet BC in modeling slanted walls is somewhat different from that for straight walls. Two possible implementations are investigated, which are: 1) single-face off-grid Dirichlet BC—when the off-grid wall within a cell consists of one face, as shown in Fig. 7 and 2) double-face off-grid Dirichlet BC—when the off-grid wall within a cell consists of two orthogonal faces, as shown in Fig. 8.

When the single-face Dirichlet BC is applied, as in Fig. 7, the E_y-component just outside the off-grid face is expressed through the neighboring internal E_y-component using (4) with $i=n$. This is done in the same way as in the case of straight walls. Note that the other component parallel to the off-grid PEC wall—in this example, E_z—cannot be expressed using (4) from its nearest neighbor if it equals zero. Equation (9) is then used with $s=2$. Alternatively, the weighted sum (11) may be used regardless of the value of the closest component. Assigning nonzero values to the two (external) components parallel to the off-grid PEC face is necessary as they participate in the calculations of the magnetic-field components.

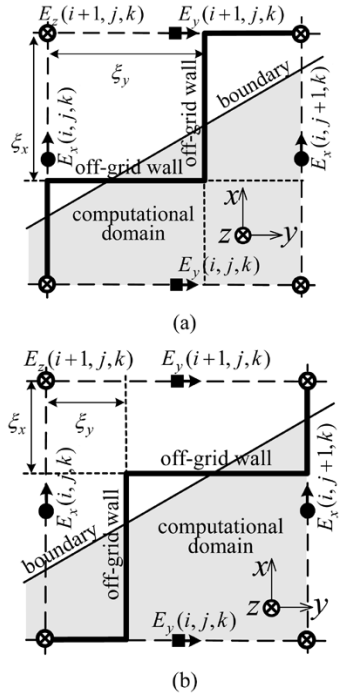

Fig. 8. Numerical cell showing the application of double-face off-grid BCs for a staircase approximation. The component $E_x(i,j,k)$ is expressed through $E_x(i,j+1,k)$ using (8) with $j=n$, $s=1$, $\xi=\xi_y$. The component $E_y(i+1,j,k)$ is expressed through $E_y(i,j,k)$ using (8) with $j=n$, $s=1$, and $\xi=\xi_x$. The component $E_z(i+1,j,k)$ is not needed. Two versions are possible: (a) $\xi_x>0.5$ and $\xi_y>0.5$ or (b) $\xi_x<0.5$ and $\xi_y<0.5$.

When the double-face off-grid Dirichlet BC is applied, as in Fig. 8, for the E_y-component, (3) or (8) is used with $\xi=\xi_x$; for the E_x-component, (3) or (8) is used with $\xi=\xi_y$. The E_z-component is parallel to both off-grid boundaries, but it is not needed, as there are two tangential E-field components already defined in the boundary cell—E_x and E_y.

Here, it is important to note that both $E_x(i,j,k)$ and $E_y(i+1,j,k)$ have to remain external to the off-grid staircase. Therefore, looking from the exterior cell corner, the off-grid boundaries within a given cell must be either: 1) both at a distance greater than one-half grid step ($\xi_x>0.5$ and $\xi_y>0.5$) or 2) both at a distance smaller than one-half grid step ($\xi_x<0.5$ and $\xi_y<0.5$).

2) Accuracy Improvement With the New Staircases: The conventional and modified staircase approximations of the slanted walls are compared. In Table III, the results for the first resonant frequency are shown. The relative error is 1.88% with the usual rule-of-thumb, which includes in the computational volume the boundary cells whose half-or-more volume is internal (Case A).

The proposed modification is based on a staircase with off-grid BCs applied for boundary cells of volume between 25%–75% within the slanted boundary. The choice of the offsets is discussed in Section IV-C.3.

It is well known that the largest errors in the calculations are due to the inadequate representation of edges and corners. Therefore, initially, the off-grid BCs were applied only around the corners, shown in Fig. 6 as regions A, B, A', and B' of the

TABLE III
DEPENDENCE OF THE ERROR ON THE STAIRCASE VERSION

Border cells *included* if :	$f_{TE_{011}}$ [GHz]	δ [%]
Case A: $V_{in} > 50\,\%$ (conventional staircase)	12.25647	1.880
Case B: $V_{in} > 50\,\%$, plus single-face off-grid BC at corners	12.35721	0.946
Case C: $V_{in} > 50\,\%$ plus double-face off-grid BC at corners	12.41572	0.477
Case D: $V_{in} > 75\,\%$, plus double-face off-grid BC at all cells where V_{in} =25-75 %	12.48959	0.014

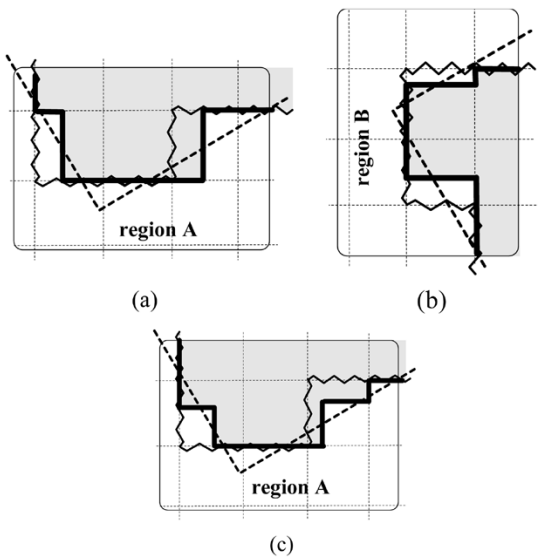

Fig. 9. (a) and (b) Modification of regions A and B using a single-face off-grid Dirichlet BC (Case B). (c) Modification of region A using a double-face off-grid Dirichlet BC (Case C).

cross section. Two versions are shown in Fig. 9. In the first version [see Fig. 9(a) and (b)], a single-face off-grid Dirichlet BC is applied for each cell in the modified areas. The modifications of regions A' and B' are mirror images of those for regions A and B, respectively. The result (Case B in Table III) is a reduction of the relative error in half in comparison with the conventional staircases—to 0.946%. If double-face off-grid BCs are used in the corner regions, as in Fig. 9(c), further reduction of the relative error results—below 0.5% (Case C in Table III). If the double-face BC is applied to all boundary cells with volume between 25%–75% inside the boundary, as shown in Fig. 10, the relative error drops to 0.014%. Simulations with 200 000 time steps have been performed and no late time instabilities have been observed.

3) Choice of the Offsets for Off-Grid Dirichlet BC: The position of the off-grid boundaries is chosen as follows. Denote the normalized internal volume of a boundary cell as $V_{\rm in}$. Clearly, $0 \le V_{\rm in} \le 1$. The replacement of the actual slanted boundary with the double-face off-grid boundary should leave the internal volume in the modified staircase approximation the same as the original internal volume (with the slanted boundary). In the case

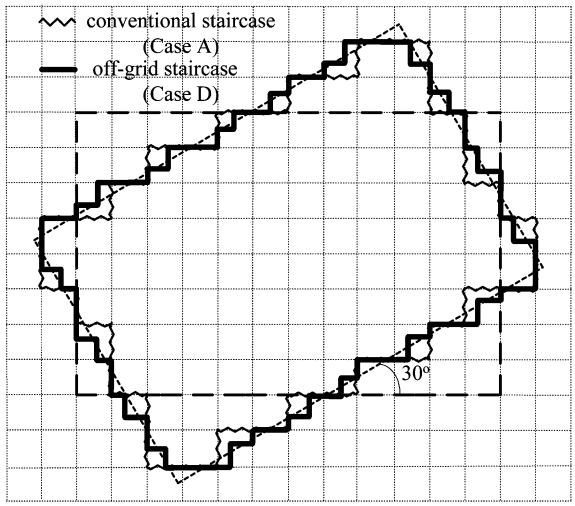

Fig. 10. Modification of the staircase from Fig. 4 at all boundary cells of internal volume between 25%–75% using a double-face off-grid Dirichlet BC.

of the double-face off-grid BC, this leads to the following constraint (see Fig. 8):

$$\begin{aligned} 1 - V_{\rm in} &= \xi_x \xi_y, \qquad \text{for } \xi_x > 0.5; \quad \xi_y > 0.5 \\ V_{\rm in} &= (1-\xi_x)(1-\xi_y), \qquad \text{for } \xi_x < 0.5; \quad \xi_y < 0.5. \end{aligned} \tag{20}$$

The most straightforward choice for the offsets is

$$\begin{aligned} \xi_x = \xi_y &= 1 - \sqrt{V_{\rm in}}, \qquad \text{for } 0.25 < V_{\rm in} < 0.4375 \\ \xi_x = \xi_y &= \sqrt{1 - V_{\rm in}}, \qquad \text{for } 0.4375 \le V_{\rm in} < 0.75. \end{aligned} \tag{21}$$

This is the preferred choice because it is: 1) programmable—easy to implement in a subroutine before the time stepping begins; 2) robust—insensitive to rounding errors in the calculation of the volume $V_{\rm in}$ of the boundary cells; 3) accurate—leads to very accurate results; and 4) stable—when applied for boundary cells of $0.25 < V_{\rm in} < 0.75$. The boundary cells of $V_{\rm in} \le 0.25$ are entirely excluded and those of $V_{\rm in} \ge 0.75$ are entirely included in the staircase approximation.

Fig. 11 presents the graph of the recommended offsets (21) for $0.25 < V_{\rm in} < 0.75$ with the bold solid lines (b). The value $V_{\rm in}^* = 0.4375$ corresponds to $\xi_x = \xi_y = 0.75$, which is the upper limit of the offset for stable staircases with double-face off-grid BCs.

The same reasoning as above is applied for the offset with single-face off-grid BCs: the internal volume of the boundary cell remains intact in the staircase approximation. This natural requirement leads to

$$\xi = 1 - V_{\rm in}, \qquad 0 < V_{\rm in} < 1. \tag{22}$$

We note that when single-face off-grid BCs are used for slanted walls, if $s = 1$ is used in (8), the corresponding upper limit of the offset for stable staircases is set to $\xi_{\max}$, as given by (7), e.g., for $\xi_{\max} = 0.85$ (i.e., $V_{\rm in} > 0.15$) $c_{\rm CFL} = 0.88$, although values as high as $\xi_{\max} = 0.90$ (i.e., $V_{\rm in} \ge 0.10$) for corner boundary cells still preserve stability. If one needs to apply an off-grid BC for $V_{\rm in} < 0.15$, $s = 2$ must be used in (8). Naturally, using the weighted sum (11) instead of (8) is a better choice for two reasons, which are: 1) it gives stable results for any offset ξ (we recall that the value of $\xi_{\max}$ obtained from (7)

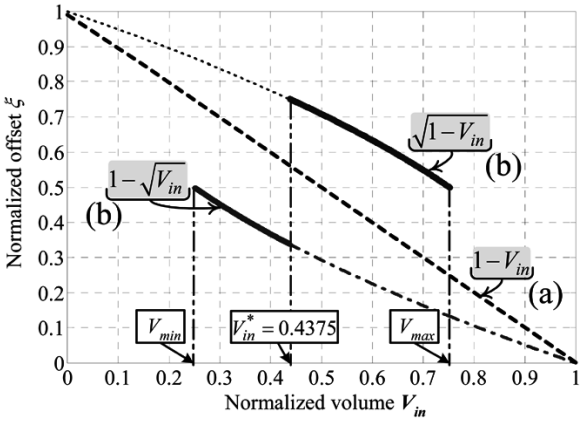

Fig. 11. Choice of normalized offsets. (a) Boundary cells of internal volume $0 < V_{\rm in} < 1$ using a single-face off-grid Dirichlet BC (dash line). (b) Boundary cells of internal volume between $V_{\rm min} = 0.25$ and $V_{\rm max} = 0.75$ using a double-face off-grid Dirichlet B: preferred choice for the offsets (bold solid lines), possible, but not recommended choice (dashed–dotted line), unstable solution (dotted line).

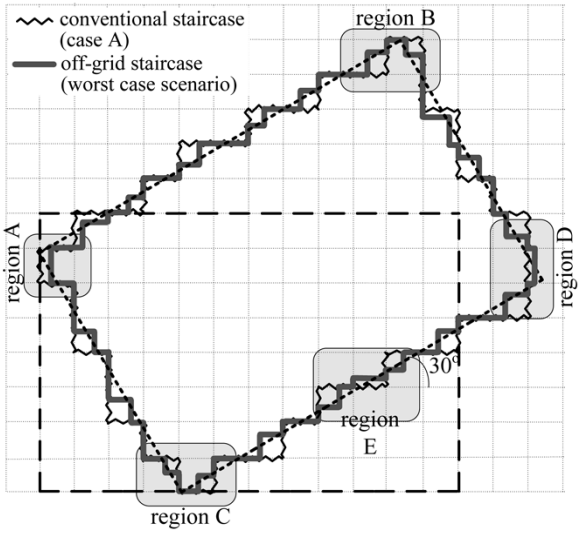

Fig. 12. "Worst case scenario": the rotated resonator has corner(s) at or near grid nodes. The proposed modification of the conventional staircase is applied at all boundary cells of internal volume between 20%–80%. A double-face off-grid BC is used for most boundary cells. In regions A, D, and E, a combination of a single- and double-face off-grid BC is applied.

is embedded in this formula) and 2) it holds regardless of the value of the closest field component (which may be zero in the staircase approximation).

The graph of the single-face offset (22) is shown in Fig. 11 with the dashed line (a). Single face off-grid BC is not the recommended choice for slanted walls, as it is not robust: the accuracy is sensitive with respect to the choice of the off-grid boundary direction and offset. However, it is very well suited for the corner cells at the intersection of slanted walls.

4) Accuracy and Stability Considerations: The stability range of the single-face off-grid Dirichlet BC is $0 < V_{\rm in} < 1$. The stability range of the double-face off-grid Dirichlet BC is $0.25 \leq V_{\rm in} < 1$.

For most applications, to keep the relative error below 0.1% $(-60$ dB$)$, it is enough to modify the staircase with an off-grid BC at all boundary cells with $V_{\rm in} = 0.50 \pm 0.25$ using the double face off-grid Dirichlet BC.

In the case when the highest possible accuracy is required (relative error of the order 0.01%), one may use the off-grid BCs for all boundary cells up to $V_{\rm in} = 0.50 \pm 0.35$.

- For boundary cells with $0.75 = V_{\rm max} < V_{\rm in} < 0.85$, one may use either the single-face off-grid BC (22) or the double-face off-grid BC with $\xi_x = \xi_y = 1 - \sqrt{V_{\rm in}}$. Cells with $V_{\rm in} > 0.85$ are entirely included in the computational domain.
- For boundary cells with $0.15 \leq V_{\rm in} < V_{\rm min} = 0.25$, one may use the single-face off-grid BC (22). The boundary cells with $V_{\rm in} < 0.15$ are entirely excluded from the computational domain.

5) Discussion and Illustrative Results: To summarize, the highest accuracy is obtained when for all boundary cells with $V_{\rm in}$ in the range (0.15, 0.85), the double-face off-grid BC is used where possible, and the single-face off-grid BC at those locations where the double-face off-grid BC cannot be applied. An example of such a situation is "the worst case scenario" for the rotated cavity, where one or more corners are in very close proximity to or coincide with grid nodes. The conventional staircase approximation then gives the highest relative errors. In Fig. 12, such a rotated and translated resonator is shown, together with its conventional staircase approximation and the proposed modified staircase. The dimensions of the resonator and the discretization are the same as above.

One may notice a few important implementation details as follows.

1) In corner region A of the rotated cross section, only a single-face off-grid BC can be applied, as there is only one nonzero internal field component in the cell and, therefore, the offset is chosen using (22).
2) In regions B and C, double-face off-grid BCs are applied in adjacent cells, and the offsets in each cell are chosen using (21).
3) In region D, a combination of single- and double-face off-grid BCs is applied. The corner cells are preferably always modeled with an off-grid BC, even if the offset is $\xi > 0.85$, in which case, either (11) is used or (8) with $s = 2$.
4) In region E, double-face off-grid BCs can be applied to the first and third cells, but only a single-face off-grid BC can be applied in the middle cell. The reason is that the middle and right cells have the same row index. Hence, one of the tangential-field components, the E_x component in this case, remains in the interior of the computational domain—see $E_x(i, j+1, k)$ in the example in Fig. 8(b) and, therefore, cannot be used as the second external component for a double-face off-grid BC.

The combination of single- and double-face off-grid BCs occurs more frequently for smaller angles of rotation—in adjacent boundary cells sharing the same row or column index.

To summarize, the most important considerations when dealing with slanted walls are: 1) to ensure that the field values at external nodes are not used for calculations in two adjacent boundary cells; 2) there is one nonzero internal tangential E-field component in order to apply a single-face off-grid BC [see Fig. 13(a)]; or 3) there are two nonzero internal tangential E-field components (orthogonal to each other) in order to apply a double-face off-grid BC [see Fig. 13(b)].

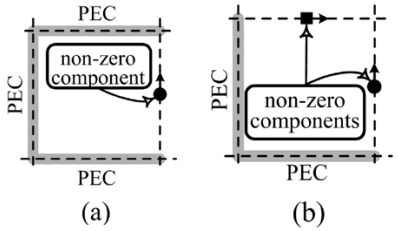

Fig. 13. (a) Boundary cell with a single nonzero internal tangential E-field component. (b) Boundary cell with two nonzero internal tangential E-field components.

TABLE IV
DEPENDENCE OF THE RELATIVE ERROR ON THE ANGLE OF ROTATION

	Conventional staircase		Off-grid staircase	
Angle of rotation	$f_{TE_{011}}$ [GHz]	δ [%]	$f_{TE_{011}}$ [GHz]	δ [%]
0^0	12.475204	0.1291	(on-grid BC)	
20^0	12.103940	3.1014	12.507696	0.1308
30^0	12.256474	1.8803	12.494389	0.0243
30^0 (worst case, Fig. 12)	12.016641	3.8003	12.483837	0.0602
40^0	11.971552	4.1613	12.484797	0.0525
45^0	12.051177	3.5238	12.503983	0.1011

In the case of a combination of single- and double-face off-grid BCs in neighboring cells, the above constraints are dealt with as follows.

Noninterference Rule: Let the internal volumes of two adjacent boundary cells having the same row or column index be $0.25 < V_{\text{in}}^{(1)} < V_{\text{in}}^{(2)} < 0.75$. In order that the assigned external field values in each cell *do not to interfere with each other*, the double-face off-grid BC must be applied in the cell of the lesser volume $V_{\text{in}}^{(1)}$ and the single-face off-grid BC must be applied in the cell of the greater volume $V_{\text{in}}^{(2)}$.

In the Appendix, we outline an algorithm for the sequence of steps when implementing off-grid BCs for slanted walls.

When the rotated resonator in Fig. 12 is approximated with the conventional staircase, the relative error for $f_{\text{TE}_{011}}$ is 3.80%. With the proposed modification applied to boundary cells with $0.20 < V_{\text{in}} < 0.80$, the relative error is reduced by two orders of magnitude, i.e., to 0.06%. No late time instabilities have been observed (in simulations with 200 000 time steps). Next, in order to observe how the error depends on the angle of rotation, the same resonator has been rotated at different angles. The relative errors in the calculated first resonant frequency using the conventional staircase and the proposed modification with respect to the analytical value are compared in Table IV. In all cases, the relative error of the proposed staircase with an off-grid Dirichlet BC is no more than 0.13%, which is the accuracy of the calculations with on-grid boundaries.

D. Modeling of Curved PEC Walls

The accuracy of the proposed method in modeling curved PEC walls has been investigated by applying it to a cylindrical resonator. The curved PEC walls have been modeled by a conventional staircase and by a modified staircase applying the off-grid Dirichlet BCs.

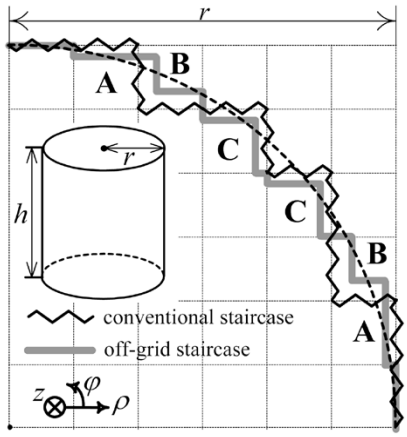

Fig. 14. Quarter cross section of the cylindrical resonator. The modified staircase uses a single-face off-grid Dirichlet BC at cell A and a double-face off-grid Dirichlet BC at cells B and C.

First, the resonator of radius $r = 7.5$ mm and height $h = 20$ mm has been modeled by the standard FDTD algorithm on a uniform grid of $\Delta x = \Delta y = \Delta z = 1.25$ mm with $c_{\text{CFL}} = 0.866$. The conventional staircase includes in the computational domain the boundary cells with an internal volume of 50% or more. The analytical value of the dominant resonant frequency is $f_{\text{TE}_{111}} = 13.905912$ GHz.

Using the conventional staircase, the calculated frequency is 13.696 438 GHz, which represents a relative error of 1.51%.

A combination of single-face and double-face off-grid Dirichlet BCs has then been applied, as shown in Fig. 14. Due to the symmetry, only one-quarter of the cross section of the cylindrical resonator is shown. At cell A, the single-face off-grid Dirichlet BC (22) is applied; at cells B and C, the double-face off-grid Dirichlet BC is applied using offsets

$$\begin{aligned} \xi_x = \xi_y &= \sqrt{1 - V_{\text{in}}}, && \text{for } V_{\text{in}} \in (0.34, 0.75) \ \{\text{cells B}\} \\ \xi_x = \xi_y &= 1 - \sqrt{V_{\text{in}}}, && \text{for } V_{\text{in}} \in (0.25, 0.34) \cup (0.75, 0.9) \\ & && \{\text{cells C}\}. \end{aligned} \tag{23}$$

Here, we note that, when modeling curved walls, the stability region for $\xi_x = \xi_y > 0.5$ is up to $\xi_{\max} = 0.8$, which corresponds to $V_{\text{in}} = 0.34$, i.e., for $V_{\text{in}} \in (0.34, 0.75)$, the upper part of curve (b) in Fig. 11 is used.

The calculated resonant frequency of TE_{111}, 13.893 102 GHz, has a relative error of 0.092%, a value lower by an order of magnitude in comparison with the conventional staircase. Similarly, for the TM_{110} mode, the analytical resonant frequency is 24.376 484 22 GHz and with the proposed off-grid staircase, the calculated frequency is 24.392 073 GHz, i.e., a relative error of 0.064%, while with the conventional staircase, the relative error is 0.680% (the calculated frequency is 24.210 758 2 GHz).

V. CONCLUSION

A simple novel method to implement off-grid PEC and PMC walls within the FDTD method has been proposed. The method

is easy to incorporate into existing standard FDTD codes. It features very high accuracy and has a negligible computational impact. The proposed off-grid boundaries significantly improve the flexibility of the FDTD method while preserving the spatial and time steps. Thus, the accuracy of subgridding is achieved without its complexity and computational cost. Examples of parallel, slanted, and curved off-grid boundary walls have been shown. Although the slanted walls are misaligned in two dimensions with respect to the existing grid in our examples, the method can be easily extended to three-dimensional (3-D) misalignments. For slanted and curved walls, combinations of single- and double-face off-grid BCs have been proposed, and a robust algorithm for the choice of the offsets has been given. Further applications of the method in structures containing knife edges and corners are currently investigated.

APPENDIX

The algorithm to implement off-grid BCs for slanted walls can be summarized as follows.

1) Calculate the internal volume V_{in} of all boundary cells in the same way as done for the conventional FDTD.
2) Record the boundary data for each slanted wall, e.g., in the form of arrays with columns

$$\text{Wall\_}N = \{\, i \quad j \quad k \quad V_{\text{in}} \quad \text{flag} \quad ksi \,\}$$

where the flag values are
x: cell entirely excluded;
o: cell entirely included;
d: double-face off-grid BC;
s: single-face off-grid BC.
All offsets are initialized as $ksi = 0$.

All flags are initialized as flag $= o$ and the corresponding (boundary) tangential E-field components are zeroed. This corresponds to a conventional staircase where all boundary cells are included in the staircase approximation. Thus, assigning off-grid BC for some boundary cells will simply rewrite exterior zeroed values.

3) Given Courant factor c_{CFL}, calculate the corresponding $\xi_{\max}$ and $\xi_{\min} = 1 - \xi_{\max}$ using (7), and from there—the range for the boundary cell volumes $[V_{\min}, V_{\max}]$ where off-grid BC will be applied.
4) For all boundary cells

$$\text{If } V_{\text{in}} < V_{\min} \text{ then flag} = x.$$

5) For all cells with flag $= x$, assign zero values to the corresponding (new boundary) tangential E-field components.
6) For the corner cells: if two nonzero internal E-field components are available, then flag $= d$, else flag $= s$ (see Fig. 13).
7) For each wall: compare the row/column indexes of all adjacent boundary cells with $V_{\min} < V_{\text{in}} < V_{\max}$. For the boundary cell couples having the same row or column index, apply the *noninterference rule*: compare their volumes, assign flag $= d$ for the cell of lesser volume and flag $= s$ for the cell of bigger volume.
8) Assign the offsets for all cells with flag $= d$: if $V_{\text{in}} < 0.4375$, apply the first formula in (21), else apply the second formula in (21).
9) Assign the offsets for all cells with flag $= s$ using (22).
10) For all cells with flag $= d$, apply the off-grid BC (8) with $s = 1$ to the corresponding tangential-field components.
11) For all cells with flag $= s$, apply (11) to the corresponding tangential-field components.

REFERENCES

[1] K. S. Yee, "Numerical solution of initial boundary value problems involving Maxwell's equations in isotropic media," *IEEE Trans. Antennas Propag.*, vol. AP-14, no. 3, pp. 302–307, May 1966.
[2] A. Taflove, *Advances in Computational Electrodynamics: The Finite Difference Time Domain Method*. Boston, MA: Artech House, 1997.
[3] C. J. Railton and J. B. Schneider, "An analytical and numerical analysis of several locally conformal FDTD schemes," *IEEE Trans. Microw. Theory Tech.*, vol. 47, no. 1, pp. 56–66, Jan. 1999.
[4] S. Dey and R. Mittra, "A locally conformal finite-difference time-domain (FDTD) algorithm for modeling three-dimensional perfectly conducting objects," *IEEE Microw. Guided Wave Lett.*, vol. 7, no. 9, pp. 273–275, Sep. 1997.
[5] C. J. Railton, I. J. Craddock, and J. B. Schneider, "The analysis of general two-dimensional PEC structures using a modified CPFDTD algorithm," *IEEE Trans. Microw. Theory Tech.*, vol. 44, no. 10, pp. 1728–1733, Oct. 1996.
[6] K. H. Dridi, J. S. Hesthaven, and A. Ditkowski, "Staircase-free finite-difference time-domain formulation for general materials in complex geometries," *IEEE Trans. Antennas Propag.*, vol. 49, no. 5, pp. 749–756, May 2001.
[7] J. Anderson, M. Okoniewski, and S. S. Stuchly, "Subcell treatment of 90° metal corners in FDTD," *Electron. Lett.*, vol. 31, pp. 2159–2160, 1995.
[8] Y. S. Rickard and N. K. Nikolova, "Off-grid perfect BC's for the FDTD method," in *Proc. Applied Computational Electromagnetics Soc. Conf.*, Syracuse, NY, 2004 [CD ROM].
[9] F. J. Harris, "On the use of windows for harmonic analysis with the discrete Fourier transform," *Proc. IEEE*, vol. 66, no. 1, pp. 51–83, Jan. 1978.

Yotka S. Rickard (M'98) received the Dipl. Eng. degree from the Technical University of Sofia, Sofia, Bulgaria, in 1976, and the M.Sc. degree in mathematics and Ph.D. degree in electrical engineering from McMaster University, Hamilton, ON, Canada, in 1997 and 2002, respectively.

Since 2003, she has been with the Natural Sciences and Engineering Research Council of Canada (NSERC) and with the Canadian Space Agency (CSA), during which time she has been with the Computational Electromagnetics Laboratory, McMaster University, Hamilton, ON, Canada. Her research interests include numerical analysis of time-dependent partial differential equations, computational electromagnetics and photonics, and computer-aided modeling of microwave to optical-wave structures.

Dr. Rickard was the recipient of an NSERC Post-Doctoral Fellowship.

Natalia K. Nikolova (S'93–M'97) received the Dipl. Eng. degree from the Technical University of Varna, Varna, Bulgaria, in 1989, and the Ph.D. degree from the University of Electro-Communications, Tokyo, Japan, in 1997.

From 1998 to 1999, she was with the Natural Sciences and Engineering Research Council of Canada (NSERC), during which time she was initially with the Microwave and Electromagnetics Laboratory, DalTech, Dalhousie University, Halifax, NS, Canada, and then for a year with the Simulation Optimization Systems Research Laboratory, McMaster University, Hamilton, ON, Canada. In July 1999, she joined the Department of Electrical and Computer Engineering, McMaster University, where she is currently an Associate Professor. Her research interests include theoretical and computational electromagnetism, high-frequency analysis techniques, as well as computer-aided design (CAD) methods for high-frequency structures and antennas.

Dr. Nikolova was the recipient of an NSERC Post-Doctoral Fellowship from 1998 to 1999. She currently holds an NSERC University Faculty Award, which she was the recipient of in 2000 and 2003, respectively.